Monitoring Dynamic Cellular Redox Homeostasis Using Fluorescence-Switchable Graphene Quantum Dots

Nan Li,[1] Aung Than,[1] Chencheng Sun,[2] Jingqi Tian,[1] Jie Chen,[1] Kanyi Pu,[1] Xiaochen Dong,[2] Peng Chen*[1]*

[1] Division of Bioengineering, School of Chemical & Biomedical Engineering, Nanyang Technological University, 70 Nanyang Drive, Singapore 637457

[2] Key Laboratory of Flexible Electronics (KLOFE) & Institute of Advanced Materials (IAM), Jiangsu National Synergetic Innovation Center for Advanced Materials (SICAM), Nanjing Tech University (NanjingTech), 30 South Puzhu Road, Nanjing 211816, China

*Corresponding to: chenpeng@ntu.edu.sg or iamxcdong@njupt.edu.cn

ABSTRACT: Monitoring cellular redox homeostasis is critical to the understanding of many physiological functions ranging from immune reactions to metabolism, as well as to the understanding of pathological development ranging from tumorigenesis to ageing. Nevertheless, there is currently lack of appropriate probes for this ambition, which should be reversibly, sensitively, and promptly responsive to a wide range of physiological oxidants and reductants. In this work, a redox-sensitive fluorescence-switchable probe is designed based on graphene

quantum dots (GQDs) functionalized with chelated redox Fe^{2+}/Fe^{3+} couple. The underlying mechanism is investigated and discussed. The high sensitivity and fast response are attributable to the fact that the GQD's photoluminescence is highly sensitive to photon-induced electron transfer because of its ultra-small size and associated prominent quantum confinement effect. Also taking advantages of GQD's excellent photostability, biocompatibility, and readiness for cell uptake, our reversibly tunable fluorescence probe is employed to monitor in real-time the triggered dynamic change of the intracellular redox state. This addition to the limited arsenal of available redox probes shall be useful to the still poorly understood redox biology, as well as for monitoring environment or chemical processes involving redox reactions.

KEYWORDS: *graphene quantum dots • redox homeostasis • fluorescent probes • live cell imaging*

Endogenously produced reactive oxygen species (ROS), being inevitable metabolic byproducts, are implicated intriguingly in cell fate decisions and signal transduction pathways.[1, 2] But oxidative stress caused by excess ROS leads to tissue damage and various undesired physiological consequences. On the other hand, various biologic antioxidants or reductants scavenge free ROS to prevent oxidative stress.[3] Nevertheless, high reductive stress is also cytotoxic. Hence, proper cell functions critically depend on the balanced intracellular redox environment, namely cellular redox homeostasis.[4, 5] The redox imbalance is implicated in a wide range of pathological conditions, including neurodegenerative diseases,[6, 7] chronic kidney disease,[8] diabetes,[9] cancers,[10] and ageing.[11] The cellular redox dynamics and its regulations, however, are still largely elusive because of the lack of effective tools to reveal it in real-time at single cell or subcellular levels.

Sensitive probes capable of monitoring cellular redox homeostasis are instrumental to the understanding of many physiological functions ranging from immune reactions to metabolism, as well as to the understanding of pathological development ranging from tumorigenesis to aging. Conventional redox measurements (*e.g.*, enzymatic assays, electrochemical analyses, high performance liquid chromatography and surface enhanced Raman spectroscopy) are usually disruptive, slow, and only able to report ensemble static behavior from cell populations.[12-14] To tackle these issues, a number of oxidation or reduction sensitive fluorescence probes based on naturally encoded proteins, synthesized organic molecules or semiconductor quantum dots have been developed.[15-17] But these probes often suffer from the problems of poor photostability, cytotoxicity, insufficient sensitivity, poor solubility, difficult synthesis, or irreversible responsiveness. Graphene quantum dots (GQDs), which are nanometer-sized and atomically-thin planar graphitic carbon structures, recently emerge as superior fluorophores for bioimaging and optical sensing because of their unique combination of several key merits, including tunable photoluminescence (PL), molecular size, excellent photostability, good water solubility, chemical inertness, biocompatibility, ease to be functionalized, readiness to be internalized by cells, and low cost.[18-28]

Most redox probes are selectively responsive to certain redox species, which are useful for the purposes of investigating specific redox pathways.[29, 30] Here, we hope to devise a strategy to visualize the overall cellular redox state and its dynamic change in the context of physiological events using switchable fluorescence probes. We conceive that GQDs functionalized with moieties possessing reversible redox states at a small-valued potential are highly suitable for the purpose. Benefiting from the extremely small size of GQDs, fluorescence quenching effect due to photo-induced electron transfer (PET) from GQD to the attached electron-withdrawing redox

moieties shall be much more prominent than other fluorescence reporters.[31, 32] According to PL quenching and recovery, redox state and its change may be conveniently, continuously, and reversibly gauged.

Based on the aforementioned rationales, we confer GQD with redox Fe^{2+}/Fe^{3+} couple by conjugating it with iron chelating group – desferrioxamine B (DFOB). Fe^{2+}/Fe^{3+} has a low standard redox potential of E_0 = 0.769 V, rendering it responsive to a wide range of reactions which have an oxidation potential >0.769 V or a reduction potential <0.769 V. In fact, Fe^{2+}/Fe^{3+} couple is the enzyme cofactor important to the redox chemistry in nearly all living organisms. We demonstrate that GQD-DFOB-Fe^{2+} can be used to detect various ROS based on PL quenching while GQD-DFOB-Fe^{3+} can be used to detect antioxidants based on PL recovery (Figure 1), even at extremely low concentrations. The underlying mechanism is investigated and discussed. Furthermore, fluorescence-switchable GQD-DFOB-Fe^{2+}/Fe^{3+} is employed to resolve the dynamic changes of the intracellular redox state in response to physiological stimuli.

RESULTS AND DISCUSSION

GQDs were readily synthesized by chemical exfoliation from carbon black as previously reported.[33, 34] The quantum yield of the purified GQDs is measured to be ~12.3% (at pH 7.0) using Rhodamine 6G as the reference.[35] The average diameter of GQDs is ~2.55 nm (± 0.32 nm, 209 samples) with a narrow size distribution (Figure 2A). The graphitic lattice of GQD can be clearly resolved under high-resolution TEM image (Figure 2B), showing good crystallinity with ~0.245 nm lattice spacing which corresponds to (1120) lattice fringes of graphene. The average thickness of GQDs revealed by the atomic force microscopy (AFM) image (Figure 2C) is ~0.7 nm (±0.16 nm, 154 samples), indicating that they are mostly single-atom-thick. The GQD

aqueous dispersion shows high stability without obvious aggregation observed after months because these GQDs bear abundant oxygen-containing functional groups. The maximum fluorescence emission from GQDs is achieved at ~527 nm while being excited at 450 nm (Figure 2D). Therefore, this pair of emission and excitation wavelengths is used for the following experiments. The excitation spectrum of our GQDs shows two peaks corresponding to the σ-π and π-π* transitions originating from the carbene-like triplet state of the zig-zag edges of GQDs (Figure S1 in the Supporting Information). DFOB is an iron chelator which is clinically used to treat iron overload disorders (*e.g.*, hemochromatosis).[36] It is covalently conjugated on GQD *via* the formation of amide bonds between the carboxyl groups on GQD and the primary amino groups on DFOB. Owing to the high association constants (or stability constants) to both ferrous ion ($K_{a,\,Fe2+} = 10^{21.2}$ or $pK_{a,\,Fe2+} = 21.2$) and ferric ion ($K_{a,\,Fe3+} = 10^{29.9}$ or $pK_{a,\,Fe3+} = 29.9$), DFOB is able to stably anchor these ions adjacent to GQD.[37]

Gel electrophoresis of purified bare GQDs yields a narrow band much below that from a 10 kDa protein marker while the band from DFOB-modified GQDs (GQD-DFOB) is also narrow and fluorescent but shows lower electrophoretic mobility because of increased molecular weight (Figure S2A in SI). These results indicate the narrow size distribution of GQDs and successful conjugation of DFOB without quenching GQD's photoluminescence. Figure S2B further confirms that the PL spectrum of GQDs is fully preserved after attaching DFOB. GQD-DFOB suspension appears light yellow under daylight and emits green fluorescence under 365 nm UV-illumination (inset of Figure S2B in SI).

As shown by Fourier transform infrared spectroscopy (FTIR), the success of DFOB conjugation on carboxyl-bearing GQD is evidenced by the diminishment of COOH peak at 1280 cm^{-1} and appearance of CO-NH peak (amide bond) at 1664 cm^{-1} (Figure S2C in SI). In addition,

X-ray photoelectron spectroscopy (XPS) demonstrates that the original bare GQDs exhibits a dominant graphitic C1s peak at ca. 285 eV, O1s peak at ca. 532 eV and N1s at ca. 400 eV. The successful conjugation of DFOB and chelation of Fe^{2+} or Fe^{3+} on GQD are corroborated by the increase of N1s peak and appearance of Fe2p peak (Figure S2D in SI). Consistently, the zeta potential of GQDs-DFOB is positively shifted to –7.02 ± 1.38 mV (n = 10) comparing with the bare carboxylated GQDs (–27.50 ± 0.96 mV, n = 10), because the negatively charged carboxyl groups originally present on GQDs are consumed to form amide bonds with DFOB. According to the size of our GQD (~2.55 nm, consisting of ~200 carbon atoms) and the atomic molar ratios of carbon and nitrogen obtained from XPS measurement (92.67% and 7.33% respectively), we estimate that ~4 DFOB molecules are conjugated on a GQD. This is a reasonable number because higher grafting density of DFOB is hindered by the steric exclusion. Dynamic light scattering (DLS) measurements show that the hydrodynamic diameters of GQD-DFOB with or without bound Fe^{3+} ions are only slightly larger than that of bare GQDs, implying that DFOB conjugation and chelation of Fe^{3+} do not cause any aggregation despite a decrease of particle charges (Figure S3 in SI).

The direct electronic bandgap (E_{GQD}) of ~2.35 eV is estimated as the ratio between the square of the absorption energy and the photo energy based on the UV-vis absorption spectrum of our GQDs (Figure S4 in SI). This value is close to the previously reported value from carboxylated GQDs with diameter ~2.6 nm.[38] As the valence band energy of GQD (E_v) is about –6.1 eV below the vacuum level,[39] its conduction band energy (E_c) is thus about $E_v + E_{GQD} = –3.75$ eV (Figure 3A). The standard reduction potential of Fe^{3+} is $E^0 = 0.769$ V vs. NHE.[40] At pH 7.0 (our experimental condition), the actual reduction potential $E_{Fe3+} = E^0 – 0.059 \times pH = – 0.356$ V. The electrochemical reduction potential can be related to the redox Fermi energy by $E_{Fe3+,red} = –4.5$

eV – E_{Fe3+} = –4.8 eV.[41, 42] Since the conductance band energy of GQD is higher than the reduction Fermi energy of Fe^{3+} ($E_c > E_{Fe3+,red}$), the photon-excited electrons in GQD will be readily transferred to nearby Fe^{3+} instead of relaxing to the ground state and emitting fluorescence. In other words, such photo-induced electron transfer (PET) causes PL quenching of GQDs. The PET coupling between GQD and Fe^{3+} is strong because the distance between GQD and DFOB chelating center is <1 nm and the free energy decrease is large (ΔG_{PET}). Specifically, $\Delta G_{PET} = E_c - E_{Fe3+,red} - E_{00} = -1.49$ eV, where E_{00} (2.54 eV) is excitation energy of GQDs determined by the intersection point between the absorption and emission spectra of GQDs (Figure S5 in SI).[31] Therefore, bonding of Fe^{3+} should lead to significant PL quenching of GQD-DFOB. Indeed, as shown in Figure 3B, loading Fe^{3+} (15 μM) onto GQD-DFOB causes ~48% of PL quenching. The possibility of GQD aggregation induced quenching is ruled out by the observation that Fe^{3+} loading does not alter the hydrodynamic diameter of GQD-DFOB reported by DLS measurement (Figure S3 in SI). Conversely, PET induced Fe^{2+} reduction is prohibited because the reduction Fermi energy of Fe^{2+} (~ –3.6 eV) is above the conduction band energy of GQD. As expected, loading Fe^{2+} onto GQD-DFOB does not cause obvious PL quenching (Figure 3B). Fe^{3+} induced PL quenching is dose dependent (Figure S6 in SI). As Fe^{3+} is a biologically important ion whose abnormal levels are associated with various diseases, GQD-DFOB can serve as sensitive fluorescence biosensor for Fe^{3+} detection with the detection limit as low as 20 nM (S/N = 3.4) and linear response range up to 15 μM (Figure S6 in SI).

When GQD-DFOB is fully loaded with Fe^{3+} (15 μM), GQD-DFOB-Fe^{3+} can be used to detect a large range of reductants based on PL recovery because when Fe^{3+} is reduced to Fe^{2+} PET caused PL quenching is relieved. As the proof-of-concept demonstration, such fluorescence turn-on detection is tested with several physiological reductants, including ascorbic acid (AA),

glutathione (GSH) and nicotinamide adenine dinucleotide hydrogen (NADH) which have a standard redox potential of –0.06,[43] –0.24,[44] and –0.32 V,[45] respectively. As shown in Figure 4A and B, the fluorescence of GQD-DFOB-Fe^{3+} enhances with increasing concentration of AA. The theoretical limit of detection (LOD) is calculated to be 2.8 nM based on LOD = 3×σ/m, where σ is the standard deviation of the response at the lowest tested concentration (100 nM here) and m is the slope of the concentration-dependent response (linear fitting in Figure 4B). Our sensor can detect GSH at 80 nM (S/N = 3.2) with the linear response range up to 20 μM (Figure S7 in the Supporting Information) and NADH at 70 nM (S/N = 3.9) with the linear response range up to 18 μM (Figure S8 in SI). The theoretical LODs for the detection of GSH and NADH are 3.3 nM and 5.6 nM, respectively. It outperforms the previously reported electrochemistry, colorimetry, fluorescence, mass spectrometry or HPLC-based methods for sensing of AA, GSH, and NADH, respectively (comparison provided in Table S1, S2 and S3 in SI).

As described earlier, Fe^{2+} does not quench GQD-DFOB. Hence, GQD-DFOB-Fe^{2+} can be employed to sense a wide range of oxidants based on PL quenching because when Fe^{2+} is oxidized to Fe^{3+} PET occurs to extinguish GQD PL. As the proof-of-concept demonstration, such fluorescence turn-off detection is tested with several physiological oxidants, including H_2O_2 and ClO^- which have standard redox potentials of 1.76 V,[46] and 1.63 V,[47] respectively. As shown in Figure 4C, a trace amount of H_2O_2 (30 nM) can be detected with a signal-to-noise ratio (S/N) of 4.3. The resulting PL quenching (at 527 nm) is linearly proportional to the H_2O_2 concentration up to ~32 μM and ~54 % quenching is obtained at this concentration (Figure 4D). The theoretical limit of detection (LOD) is calculated to be as low as 1.4 nM. Without involving usually needed enzymatic or chemical reactions, our PET-driven sensor has much faster response (within 3 min, see Figure S9 in SI) than the previously reported hydrogen peroxidase-based colorimetric,

fluorimetric, or electrochemical sensors (comparison provided in Table S4 in SI). And GQD-DFOB-Fe^{2+} is more sensitive than other H_2O_2 sensors based on different sensing modalities (comparison provided in Table S5 in SI). Similarly, ClO^- can also turn-off the PL of GQD-DFOB-Fe^{2+} in a dose-dependent manner (Figure S10 in SI), allowing detection at 25 nM with S/N = 4.5 and linear response up to 25 μM. The theoretical LOD is calculated to be as low as 2.1 nM, which is much lower than that of the previously reported fluorescence, colorimetric, or electrochemical methods (comparison provided in Table S6 in SI). To avoid PL reduction caused by spontaneous oxidation of Fe^{2+}, all the experiments were conducted with freshly prepared GQD-DFOB-Fe^{2+}. As shown in Figure S11 (SI), PL of GQD-DFOB-Fe^{2+} remains constant in ambient for hours and in deareated buffer solution for days.

Evidently, our PET-based fluorescence probe is fast and sensitive. To confirm that PET is mediated by Fe^{2+}/Fe^{3+} redox transition, XPS characterization is performed (Figure S12 in SI). In comparison with the high-resolution N1s spectrum of GQD-DFOB showing two peaks at around 401.1 and 399.2 eV corresponding to N-OH and N-H bonds (Figure S12A in SI), a new peak at ~400.3 eV corresponding to N-O-Fe coordinate bond arises after chelation of Fe^{3+} to form GQD-DFOB-Fe^{3+} (Figure S12B in SI).[48] Furthermore, the high-resolution Fe2p spectrum of GQD-DFOB-Fe^{3+} can be resolved to two distinct peaks centered at 712.2 and 726.1 eV, corresponding to the binding energies of 2p 3/2 of Fe^{3+} and 2p 1/2 of Fe^{3+}, respectively (Figure S12C in SI).[49] After the reduction of chelated Fe^{3+} by AA, as expected, the two Fe^{3+} peaks are reduced while 2p 3/2 of Fe^{2+} and 2p 1/2 of Fe^{2+} peaks become dominant (Figure S12D in SI). On the other hand, two prominent Fe^{2+} peaks (2p 3/2 peak at 710.4 eV, 2p 1/2 peak at 724.3 eV) and two weak Fe^{3+} peaks resulting from mild spontaneous oxidation in ambient condition (2p 3/2 peak at 712.2 eV, 2p 1/2 peak at 726.1 eV) can be resolved from the high-resolution Fe2p spectrum of GQD-

DFOB-Fe^{2+} (Figure S12E in SI). After exposing GQD-DFOB-Fe^{2+} to H_2O_2, the Fe2p peaks of Fe^{2+} essentially vanish because of oxidation of chelated Fe^{2+} to Fe^{3+} (Figure S12F in SI).

Neither GQD-DFOB-Fe^{3+} nor GQD-DFOB-Fe^{2+} exerts significant cytotoxicity even at the high concentration of 0.3 mg/mL (Figure S13 in SI), indicating their suitability for cell imaging. As the proof-of-concept demonstrations, we used GQD-DFOB-Fe^{2+} to monitor the increase of intracellular oxidative stress and GQD-DFOB-Fe^{3+} to monitor the rise of intracellular reductive stress in both Hela cells (a cancer cell line) and human mesenchymal stem cells (HMSC). After 1h incubation with 0.1 mg/mL GQD-DFOB-Fe^{2+} or GQD-DFOB-Fe^{3+}, numerous green puncta appear in the cytosol of both cell types, indicating the readily internalization of GQD-DFOB-Fe^{2+} or GQD-DFOB-Fe^{3+} (Figure 5A). In comparison, the cells without incubation of the probes show no fluorescence signal (Figure S14 in SI). Most internalized GQD-DFOB-Fe^{2+} or GQD-DFOB-Fe^{3+} probes are distributed throughout the cytosol (but not the nucleus) while some get into endosomes which are important sites of ROS production (Figure S15 in SI). Therefore, our probes are suitable to report the overall cellular redox states.

H_2O_2 is a common ROS produced largely by mitochondria and endosomes inside the cell and also exists extracellularly within the tissue microenvironment. It is an important signaling molecule for the regulation of many biological processes. On the other hand, an excess amount of H_2O_2 causes cell damage or triggers cell apoptosis.[50] Extracellular addition of 10 μM H_2O_2, mimic to increase the oxidative stress in the extracellular microenvironment, leads to significant PL quench of GQD-DFOB-Fe^{2+} inside both Hela cells and HMSC cells (Figure 5A and B) whereas the fluorescence signal in the untreated cells remains stable (Figure 5B). After a few minutes of delay for H_2O_2 to diffuse into the cells, PL intensity decreases continuously over time. 41.64% or 26.18% PL decrease is reached after 40 min in H_2O_2-treated Hela or HMSC

cells respectively (Figure 5B). PMA (phorbol myristate acetate) is a carcinogenic chemical (an analog to the second messenger diacylglycerol) which can potently induce a burst of cellular respiration and consequently boost production of H_2O_2 inside the cell. As shown in Figure 5A and C, after 1 h incubation of 10 μM PMA, the PL of intracellular GQD-DFOB-Fe^{2+} probes decreases by 52.64% and 28.15% in Hela and HMSC cells respectively. These experiments testify that GQD-DFOB-Fe^{2+} is able to serve as the stable and sensitive fluorescence probe to monitor induced oxidative stress in live cells in real-time. Interestingly, these experiments also suggest that the cancer cells are more susceptible to oxidative stimuli as evidenced by the faster PL decay rate of GQD-DFOB-Fe^{2+} probes in Hela cells. This is consistent with the well-accepted notion that cancer cells, which lose control of redox balance due to abnormal oxygen metabolism, usually exhibit significantly greater levels of intracellular oxidative stress,[51] and are vulnerable to additional oxidative stimulation because it pushes the already stressed cells beyond their ability to counteract through endogenous antioxidant mechanisms.[52]

Ascorbic acid (AA) and glutathione (GSH) are important antioxidants (mild reducing agents) to protect cells from oxidative stress. They play roles in cell metabolism and other functions. As shown in Figure S16A and B in the Supporting Information, the addition of 100 μM AA or GSH causes gradual fluorescence increase of GQD-DFOB-Fe^{3+} loaded Hela Cells. After 40 min, 47.54% or 38.59% PL increase is attained in AA or GSH treated cells while the PL signal in the untreated cells remains stable (Figure S16B and C in SI). Evidently, GQD-DFOB-Fe^{3+} can be employed to continuously monitor induced reductive stress in live cells.

Because Fe^{3+} and Fe^{2+} are reversible redox couple, GQD-DFOB-Fe^{3+}/Fe^{2+} is fluorescence switchable (Figure 6A). As shown in Figure 6B, its fluorescence is reversibly tunable by alternating addition of reductant (AA) and oxidant (H_2O_2) without PL degradation. Such

fluorescence-switchable redox-sensitive probe should be instrumental to monitoring the dynamic change of intracellular redox state in the context of physiological events (Figure 6C). In the experiments shown in Figure 6D, Hela cells are firstly loaded with GQD-DFOB-Fe^{3+} probes. The addition of 100 μM AA causes a continuous increase of PL intensity of the cells and subsequent addition of 10 μM H_2O_2 leads to a gradual decrease of PL intensity. As demonstrated, GQD-DFOB-Fe^{3+}/Fe^{2+} works well to report the dynamic sway from the redox homeostasis in the cell in response to physiological events.

CONCLUSIONS

In summary, a sensitive fluorescence probe for redox species is designed based on graphene quantum dots (GQDs) functionalized with chelated iron ions. The high sensitivity and fast response are attributable to the fact that the GQD's photoluminescence is highly sensitive to photo-induced electron transfer because of its ultra-small size and associated prominent quantum confinement effect. Also taking advantage of GQD's excellent photostability, biocompatibility and readiness for cell uptake, this fluorescence-switchable probe is employed to monitor in real-time the triggered dynamic changes of the overall intracellular redox status states in live cells. This addition to the limited arsenal of available redox-sensitive probes will be useful to the still poorly understood redox biology, as well as for monitoring environment or chemical processes involving redox reactions. Because GQDs are particularly sensitive to photon-induced electron transfer, similar detection mechanisms may be designed for various purposes, for example, detecting a specific oxidant or reductant.

METHODS

Synthesis and functionalization of GQDs. GQDs were prepared by refluxing carbon black powders (0.2 g) with nitric acid (50 mL, 6M) for 24 h. After centrifugation (5000 rpm for 10 min) to remove large pieces and aggregations, the sample was heat-dried to give reddish-brown powders, which were subsequently re-suspended in deionized water. The obtained suspension was then ultrafiltered twice (Amicon Ultra-4, Millipore) to retain the particles between 3 and 10 kDa.

To conjugate with DFOB, GQD solution (0.5 mg/mL) was first mixed with 1-ethyl-3-(3-dimethylaminopropyl) carbodiimide hydrochloride (10 mM; Sigma-Aldrich) and N-hydroxysuccinimide (10 mM; Sigma-Aldrich) for 20 min in borate buffer solution (10 mM, pH 5). DFOB (1 mM; Sigma-Aldrich) was subsequently added to the above mixture for reaction. After shaking for 4 h at room temperature, the mixture was supplemented with 5 mM $FeSO_4$ or $FeCl_3$ to obtain GQD-DFOB-Fe^{2+} or GQD-DFOB-Fe^{3+} respectively. After shaking for additional 30 min, the solution was then dialyzed with cellulose ester dialysis membrane (MWCO 500-1000 Da) for 48 h to remove unreacted molecules and ions (EDC, NHS, DFOB, Fe^{2+} or Fe^{3+}).

Characterizations. The morphology of synthesized GQDs was examined by transmission electron microscopy (TEM; JEM 2010, JEOL) and atomic force microscopy (AFM; MFP-3D, Asylum Research). Fourier transform infrared spectroscopy (FTIR), photoluminescence (PL) spectroscopy, UV-vis absorption spectroscopy and X-ray photoelectron spectroscopy (XPS) measurements were conducted with Bruker spectrometer (Vertex 70), and PerkinElmer fluorescence spectrometer (LS-55), Shimadzu UV-vis spectrometer (UV-245), and ESCALAB MK II X-ray photoelectron spectrometer, respectively. The zeta potentials of bare GQDs and functionalized GQDs were measured using a Malvern Zetasizer (Nano-ZS 90).

Cell imaging. The Hela cells (human epithelial carcinoma cell line; American Type Culture Collection) were cultured on Lab-Tek chambered cover-glass (Thermo Fisher Scientific) in the growth medium (DMEM supplemented with 10% fetal bovine serum and 1% penicillin–streptomycin; Life Technologies), at 37 °C in a humidified atmosphere containing 5% CO_2 and 95% air. After 1 h incubation with 0.1 mg/mL of GQD-DFOB-Fe^{3+} or GQD-DFOB-Fe^{2+}, the cells were washed and refreshed with buffer solution before being imaged (λ_{ex} = 488 nm, λ_{em} = 520 nm) with a LSM710 confocal laser-scanning microscope (Carl Zeiss, Germany). During imaging, the cells were treated with 100 μM of ascorbic acids (AA) and subsequently treated with 10 μM of H_2O_2. In some cases, the GQD-DFOB-Fe^{3+}(or Fe^{2+}) loaded cells were treated for 1 h with 10 μM PMA or 10 μM H_2O_2 or 100 μM AA or 100 μM GSH before imaging.

MTT cell viability assay. The cytotoxicity of GQD-DFOB-Fe^{2+} or GQD-DFOB-Fe^{3+} was evaluated using MTT (3-(4,5-dimethylthiazol-2-yl)-2,5-diphenyl tetrasodium bromide)-based cell viability assay (Sigma-Aldrich). Briefly, Hela cells were seeded in 96-well plates at ~3×10^5 cells per mL, and cultured in Dulbecco's modified Eagle's medium (Gibco) supplemented with 10% (v/v) fetal bovine serum at 37 °C under a humidified atmosphere containing 5% CO_2. The cells were then incubated with GQD-DFOB-Fe^{2+} or GQD-DFOB-Fe^{3+} at different concentrations for 24 h. After refreshing with the medium containing MTT reagent (0.5 mg/mL), cells were incubated for 4 h at 37 °C, followed by removal of the medium and addition of DMSO to dissolve the precipitated formazan crystal. After a brief shaking for 10 min, the amount of solubilized formazan as the indicator of cell viability was assessed by a plate reader (SpectraMax M5, Molecular Devices) at 570nm.

Polyacrylamide gel electrophoresis. GQD and GQD-DFOB (both 0.1mg/mL) in PBS buffer were electrophoretically separated through 15% polyacrylamide gel (PAGE) in Tris-glycine based

running buffer (25 mM Tris, 192 mM glycine, 0.1% SDS, pH 8) for 30 min at a constant voltage of 200 V. Spectra Multicolor broad-range protein ladder was used as the molecular weight benchmarkers. The fluorescent bands were detected in a G:Box Chemi XT4 imaging system (Syngene) at 488 nm.

ASSOCIATED CONTENT

Supporting Information. Abbreviation list; Comparison Tables to compare our method with other methods of detection of ascorbate, glutathione, NADH, H_2O_2, and ClO^-; Characterizations (PL, TEM, AFM, FTIR, electrophoresis, XPS, DLS) of GQD, GQD-DFOB and GQD-DFOB-Fe^{2+}/Fe^{3+}; PL spectra of GQD-DFOB-Fe^{3+} in response to the reductants (glutathione, NADH) and PL spectra of GQD-DFOB-Fe^{2+} in response to the oxidant (ClO^-); MTT cytotoxicity analysis; confocal imaging of the distribution of GQD-DFOB-Fe^{2+} or GQD-DFOB-Fe^{3+} probes inside the live cells and confocal monitoring of intracellular reductive stress using GQD-DFOB-Fe^{3+}. This material is available free of charge *via* the Internet at http://pubs.acs.org.

AUTHOR INFORMATION

Corresponding Author

* E-mail: chenpeng@ntu.edu.sg

Notes

The authors declare no competing financial interest.

ACKNOWLEDGMENT

This research is supported by an AcRF tier 2 grant (MOE2014-T2-1-003) from Ministry of Education (Singapore) and a start-up grant (NTU-SUG: M4081627.120) from Nanyang Technological University.

REFERENCES

1. Finkel, T. Signal Transduction by Reactive Oxygen Species. *J. Cell Biol.* **2011**, *194*, 7-15.
2. Bryan, N.; Ahswin, H.; Smart, N.; Bayon, Y.; Wohlert, S.; Hunt, J. A. Reactive Oxygen Species (ROS)--A Family of Fate Deciding Molecules Pivotal in Constructive Inflammation and Wound Healing. *Eur. Cell Mater.* **2012**, *24*, 249-265.
3. Sindhi, V.; Gupta, V.; Sharma, K.; Bhatnagar, S.; Kumari, R.; Dhaka, N. Potential Applications of Antioxidants – A Review. *J. Pharm. Res.* **2013**, *7*, 828-835.
4. Trachootham, D.; Lu, W. Q.; Ogasawara, M. A.; Valle, N. R. D.; Huang, P. Redox Regulation of Cell Survival. *Antioxid. Redox. Sign.* **2008**, *10*, 1343-1374.
5. Wang, K.; Zhang, T.; Dong, Q.; Nice, E. C.; Huang, C. H.; Wei, Y. Q. Redox Homeostasis: the Linchpin in Stem Cell Self-Renewal and Differentiation. *Cell Death Dis.* **2013**, *4*, e537.
6. Chinta, S. J.; Andersen, J. K. Redox Imbalance in Parkinson's Disease. *Biochim. Biophys. Acta-Gen Subjects* **2008**, *1780*, 1362-1367.
7. Moneim, A. E. Oxidant/Antioxidant Imbalance and the Risk of Alzheimer's Disease. *Curr. Alzheimer Res.* **2015**, *12*, 335-349.
8. Poulianiti, K. P.; Kaltsatou, A.; Mitrou, G. I.; Jamurtas, A. Z.; Koutedakis, Y.; Maridaki, M.; Stefanidis, I.; Sakkas, G. K.; Karatzaferi, C. Systemic Redox Imbalance in Chronic Kidney Disease: A Systematic Review. *Oxid. Med. Cell Longev.* **2016**, 8598253.
9. Hayden, M. R.; Sowers, J. R. Redox Imbalance in Diabetes. *Antioxid. Redox. Sign.* **2007**, *9*, 865-867.
10. Jorgenson, T. C.; Zhong, W. X.; Oberley, T. D. Redox Imbalance and Biochemical Changes in Cancer. *Cancer Res.* **2013**, *73*, 6118-6123.
11. Hagen, T. M. Oxidative Stress, Redox Imbalance, and the Aging Process. *Antioxid Redox Signal* **2003**, *5*, 503-506.
12. Rabinowitz, J. D.; Vacchino, J. F.; Beeson, C.; McConnell, H. M. Potentiometric Measurement of Intracellular Redox Activity. *J. Am. Chem. Soc.* **1998**, *120*, 2464-2473.
13. Zhu, P. J.; Oe, T.; Blair, I. A. Determination of Cellular Redox Status by Stable Isotope Dilution Liquid Chromatography/Mass Spectrometry Analysis of Glutathione and Glutathione Disulfide. *Rapid Commun. Mass. Spectrom.* **2008**, *22*, 432-440.
14. Jamieson, L. E.; Jaworska, A.; Jiang, J.; Baranska, M.; Harrison, D. J.; Campbell, C. J. Simultaneous Intracellular Redox Potential and pH Measurements in Live Cells using SERS Nanosensors. *Analyst* **2015**, *140*, 2330-2335.
15. Meyer, A. J.; Dick, T. P. Fluorescent Protein-Based Redox Probes. *Antioxid. Redox. Sign.* **2010**, *13*, 621-650.
16. Lou, Z.; Li, P.; Han, K. Redox-Responsive Fluorescent Probes with Different Design Strategies. *Accounts. Chem. Res.* **2015**, *48*, 1358-1368.
17. Kaur, A.; Kolanowski, J. L.; New, E. J. Reversible Fluorescent Probes for Biological Redox States. *Angew. Chem. Int. Ed.* **2016**, *55*, 1602-1613.

18. Baker, S. N.; Baker, G. A. Luminescent Carbon Nanodots: Emergent Nanolights. *Angew. Chem. Int. Ed.* **2010**, *49*, 6726-6744.
19. Zhu, S. J.; Zhang, J. H.; Tang, S. J.; Qiao, C. Y.; Wang, L.; Wang, H. Y.; Liu, X.; Li, B.; Li, Y. F.; Yu, W. L.; Wang, X. F.; Sun, H. C.; Yang, B. Surface Chemistry Routes to Modulate the Photoluminescence of Graphene Quantum Dots: From Fluorescence Mechanism to Up-Conversion Bioimaging Applications. *Adv. Funct. Mater.* **2012**, *22*, 4732-4740.
20. Shen, J.; Zhu, Y.; Yang, X.; Li, C. Graphene Quantum Dots: Emergent Nanolights for Bioimaging, Sensors, Catalysis and Photovoltaic Devices. *Chem. Commun.* **2012**, *48*, 3686-3699.
21. Peng, J.; Gao, W.; Gupta, B. K.; Liu, Z.; Romero-Aburto, R.; Ge, L.; Song, L.; Alemany, L. B.; Zhan, X.; Gao, G.; Vithayathil, S. A.; Kaipparettu, B. A.; Marti, A. A.; Hayashi, T.; Zhu, J.-J.; Ajayan, P. M. Graphene Quantum Dots Derived from Carbon Fibers. *Nano Lett.* **2012**, *12*, 844-849.
22. Sun, H.; Wu, L.; Wei, W.; Qu, X. Recent Advances in Graphene Quantum Dots for Sensing. *Mater. Today* **2013**, *16*, 433-442.
23. Sk, M. A.; Ananthanarayanan, A.; Huang, L.; Lim, K. H.; Chen, P. Revealing the Tunable Photoluminescence Properties of Graphene Quantum Dots. *J. Mater. Chem. C* **2014**, *2*, 6954-6960.
24. Wang, D.; Chen, J.-F.; Dai, L. Recent Advances in Graphene Quantum Dots for Fluorescence Bioimaging from Cells Through Tissues to Animals. *Part. Part. Syst. Char.* **2015**, *32*, 515-523.
25. Zheng, X. T.; Ananthanarayanan, A.; Luo, K. Q.; Chen, P. Glowing Graphene Quantum Dots and Carbon Dots: Properties, Syntheses, and Biological Applications. *Small* **2015**, *11*, 1620-1636.
26. Yoo, J. M.; Kang, J. H.; Hong, B. H. Graphene-Based Nanomaterials for Versatile Imaging Studies. *Chem. Soc. Rev.* **2015**, *44*, 4835-4852.
27. Hong, G. S.; Diao, S. O.; Antaris, A. L.; Dai, H. J. Carbon Nanomaterials for Biological Imaging and Nanomedicinal Therapy. *Chem. Rev.* **2015**, *115*, 10816-10906.
28. Bartelmess, J.; Quinn, S. J.; Giordani, S. Carbon Nanomaterials: Multi-Functional Agents for Biomedical Fluorescence and Raman Imaging. *Chem. Soc. Rev.* **2015**, *44*, 4672-4698.
29. Morgan, B.; Sobotta, M. C.; Dick, T. P. Measuring EGSH and H_2O_2 with roGFP2-based redox probes. *Free Radical Bio. Med.* **2011**, *51*, 1943-1951.
30. Jiang, X. Q.; Yu, Y.; Chen, J. W.; Zhao, M. K.; Chen, H.; Song, X. Z.; Matzuk, A. J.; Carroll, S. L.; Tan, X.; Sizovs, A.; Cheng, N. H.; Wang, M. C.; Wang, J. Quantitative Imaging of Glutathione in Live Cells Using a Reversible Reaction-Based Ratiometric Fluorescent Probe. *Acs. Chem. Biol.* **2015**, *10*, 864-874.
31. Ghosh, T.; Chatterjee, S.; Prasad, E. Photoinduced Electron Transfer from Various Aniline Derivatives to Graphene Quantum Dots. *J. Phys. Chem. A* **2015**, *119*, 11783-11790.
32. Achadu, O. J.; Nyokong, T. Interaction of Graphene Quantum Dots with 4-Acetamido-2,2,6,6-Tetramethylpiperidine-Oxyl Free Radicals: A Spectroscopic and Fluorimetric Study. *J. Fluoresc.* **2016**, *26*, 283-295.
33. Li, N.; Wang, X. W.; Chen, J.; Sun, L.; Chen, P. Graphene Quantum Dots for Ultrasensitive Detection of Acetylcholinesterase and Its Inhibitors. *2d Mater* **2015**, *2*, 034018.
34. Zheng, X. T.; Than, A.; Ananthanaraya, A.; Kim, D.-H.; Chen, P. Graphene Quantum Dots as Universal Fluorophores and Their Use in Revealing Regulated Trafficking of Insulin Receptors in Adipocytes. *ACS Nano* **2013**, *7*, 6278-6286.

35. Li, N.; Than, A.; Wang, X.; Xu, S.; Sun, L.; Duan, H.; Xu, C.; Chen, P. Ultrasensitive Profiling of Metabolites Using Tyramine-functionalized Graphene Quantum Dots. *ACS Nano* **2016**, *10*, 3622-3629.
36. Haas, K. L.; Franz, K. J. Application of Metal Coordination Chemistry to Explore and Manipulate Cell Biology. *Chem. Rev.* **2009**, *109*, 4921-4960.
37. Ussher, S. J.; Yaqoob, M.; Achterberg, E. P.; Nabi, A.; Worsfold, P. J. Effect of Model Ligands on Iron Redox Speciation in Natural Waters using Flow Injection with Luminol Chemiluminescence Detection. *Anal. Chem.* **2005**, *77*, 1971-1978.
38. Shinde, D. B.; Pillai, V. K. Electrochemical Resolution of Multiple Redox Events for Graphene Quantum Dots. *Angew. Chem. Int. Ed.* **2013**, *52*, 2482-2485.
39. Kumar, G. S.; Thupakula, U.; Sarkar, P. K.; Acharya, S. Easy Extraction of Water-soluble Graphene Quantum Dots for Light Emitting Diodes. *RSC Advances* **2015**, *5*, 27711-27716.
40. Rizvi, M. A.; Syed, R. M.; Khan, B. Complexation Effect on Redox Potential of Iron(III)−Iron(II) Couple: A Simple Potentiometric Experiment. *J. Chem. Educ.* **2011**, *88*, 220-222.
41. Bisquert, S. G. J. *Photoelectrochemical Solar Fuel Production From Basic Principles to Advanced Devices*. Springer International Publishing Switzerland 2016; 10.1007/978-3-319-2964-8, 12-13.
42. W., C. F. G. W. P. D. *Photovoltaic and Photoelectrochemical Solar Energy Conversion*. Plenum Press, New York in cooperation with NATO Scientific Affairs Division: 1980; 10.1007/978-1-4615-9233-4, 266.
43. Borsook, H.; Keighley, G. Oxidation-reduction Potential of Ascorbic Acid (Vitamin C). *Proc. Natl. Acad. Sci. U.S.A.* **1933**, *19*, 875-878.
44. Sevier, C. S.; Kaiser, C. A. Formation and Transfer of Disulphide Bonds in Living Cells. *Nat. Rev. Mol. Cell Biol.* **2002**, *3*, 836-847.
45. Matsui, T.; Kitagawa, Y.; Okumura, M.; Shigeta, Y. Accurate Standard Hydrogen Electrode Potential and Applications to the Redox Potentials of Vitamin C and NAD/NADH. *J. Phys. Chem. A* **2015**, *119*, 369-376.
46. Bockris, J. O. M.; Oldfield, L. F. The Oxidation-reduction Reactions of Hydrogen Peroxide at Inert Metal Electrodes and Mercury Cathodes. *T. Faraday Soc.* **1955**, *51*, 249-259.
47. Brown, G. M.; Gu, B. The Chemistry of Perchlorate in the Environment. In *Perchlorate: Environmental Occurrence, Interactions and Treatment*, Gu, B.; Coates, J. D., Eds. Springer US: Boston, MA, 2006; 10.1007/0-387-31113-0_2; pp 17-47.
48. Kalinowski, B. E.; Liermann, L. J.; Brantley, S. L.; Barnes, A.; Pantano, C. G. X-ray Photoelectron Evidence for Bacteria-enhanced Dissolution of Hornblende. *Geochim. Cosmochim. Ac.* **2000**, *64*, 1331-1343.
49. Kong, H.; Song, J.; Jang, J. One-step Fabrication of Magnetic Gamma-Fe_2O_3/Polyrhodanine Nanoparticles Using in-situ Chemical Oxidation Polymerization and Their Antibacterial Properties. *Chem. Commun.* **2010**, *46*, 6735-6737.
50. Lennicke, C.; Rahn, J.; Lichtenfels, R.; Wessjohann, L. A.; Seliger, B. Hydrogen Peroxide - Production, Fate and Role in Redox Signaling of Tumor Cells. *Cell Commun. Signal.* **2015**, *13*, 39-58.
51. Cairns, R. A.; Harris, I. S.; Mak, T. W. Regulation of Cancer Cell Metabolism. *Nat. Rev. Cancer* **2011**, *11*, 85-95.
52. Schumacker, P. T. Reactive Oxygen Species in Cancer Cells: Live by the Sword, Die by the Sword. *Cancer Cell* **2006**, *10*, 175-176.

FIGURES

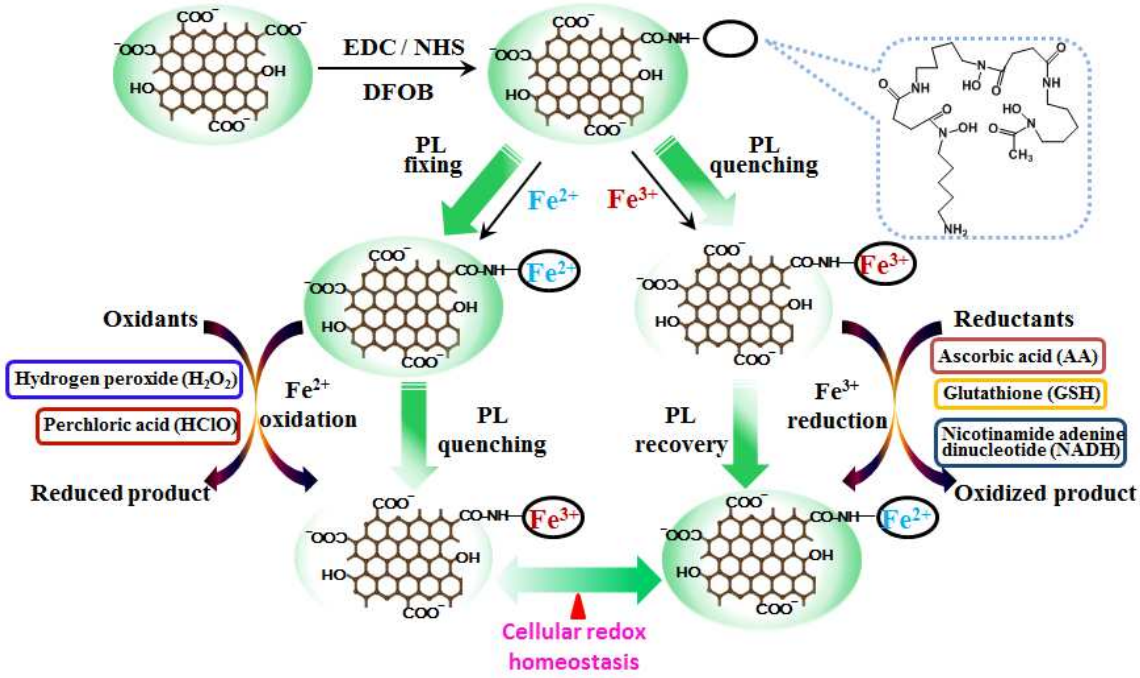

Figure 1. Schematic illustration of redox-sensitive fluorescence-switchable probe based on desferrioxamine-functionalized GQD (GQD-DFOB) chelated with redox Fe^{2+}/Fe^{3+} couple.

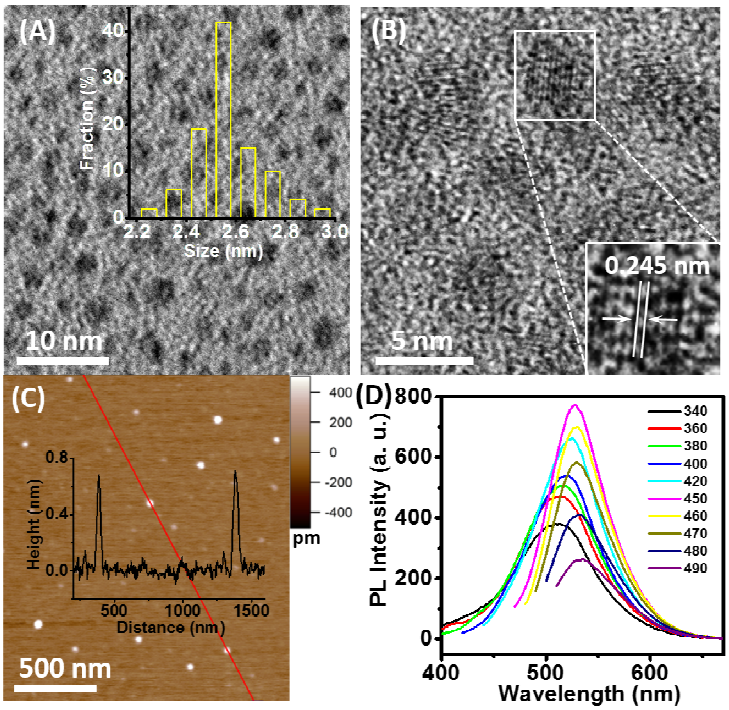

Figure 2. (A) TEM image of GQDs. Inset shows the size distribution of 209 GQDs. (B) High-resolution TEM reveals lattice spacing of GQDs. (C) AFM image of GQDs. The inset shows the height profile along the red line. (D) Photoluminescence (PL) spectra of GQD in PBS buffer solution under different excitation wavelengths (as indicated by the figure legends).

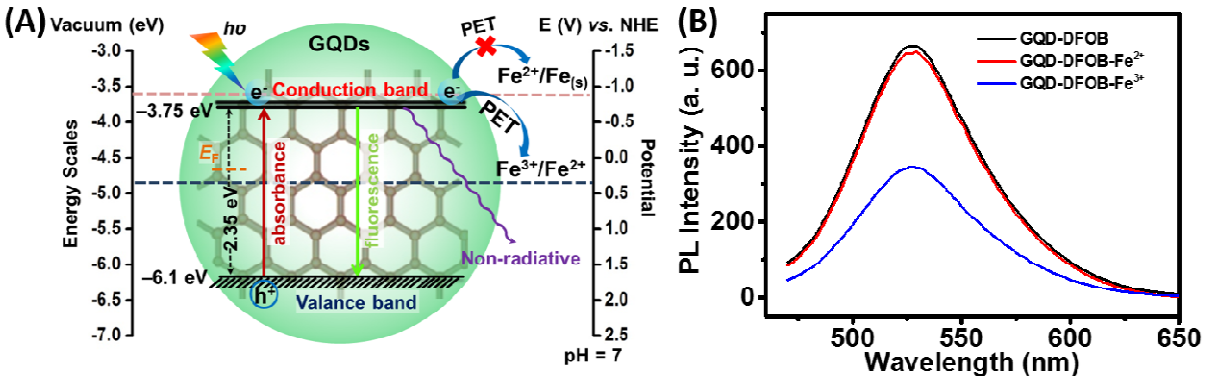

Figure 3. (A) Diagrammatic illustration of photo-induced electron transfer process between GQD and the chelated Fe^{3+}. (B) PL spectra of GQD-DFOB chelated with Fe^{2+}or Fe^{3+} (0.1 mg/mL in PBS, pH 7.0).

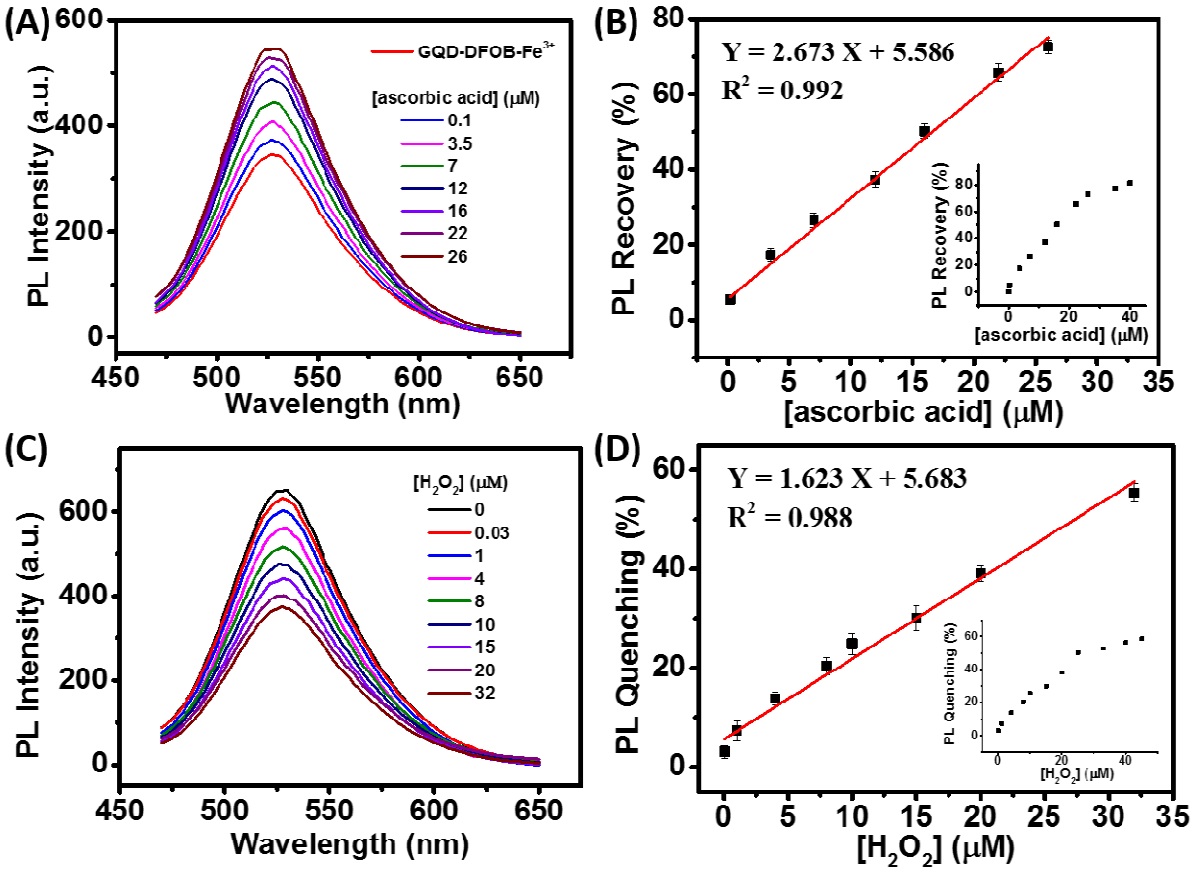

Figure 4. (A) PL spectra of GQD-DFOB-Fe^{3+} (0.1 mg/mL in PBS) in the presence of different concentrations of ascorbic acid. (B) PL quenching efficiency *vs.* ascorbic acid concentration, with linear fitting. (C) PL spectra of GQD-DFOB-Fe^{2+} in the presence of different concentrations of H_2O_2. (D) PL quenching efficiency *vs.* H_2O_2 concentration, with linear fitting. The error bars indicate the standard deviation from 3 independent measurements.

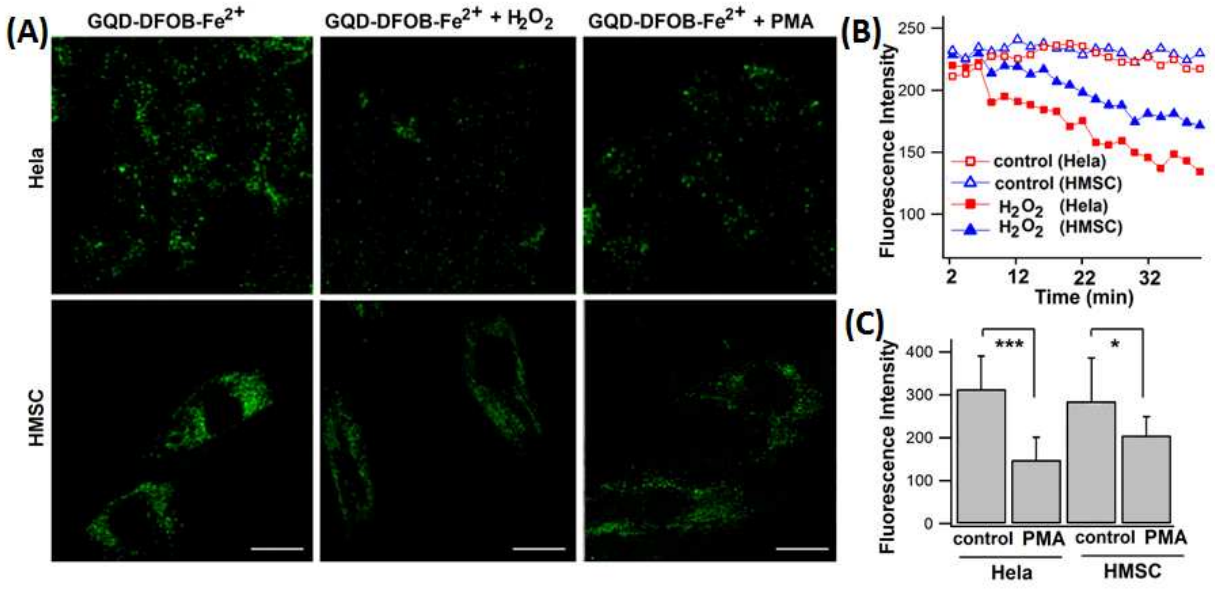

Figure 5. (A) Confocal images of Hela cells (top) and human mesenchymal stem cells (bottom) pre-incubated for 1 h with 0.1 mg/mL GQD-DFOB-Fe^{2+}, in the absence (left) or presence of 10 μM H_2O_2 for 40 min (middle) or 10 μM PMA for 1h (right). Scale bar = 10 μm. (B) The change of the averaged fluorescence intensity of 12 GQD-DFOB-Fe^{2+} loaded Hela or HMSC cells without or with 10 μM H_2O_2 stimulation (2 min interval). (C) Statistics (mean ± SD) of the fluorescence intensity of GQD-DFOB-Fe^{2+} loaded Hela or HMSC cells (n=12 - 15) in the absence or presence of 10 μM PMA for 1 h. Student's t test: *** $p < 0.001$ and * $p < 0.1$ vs. control.

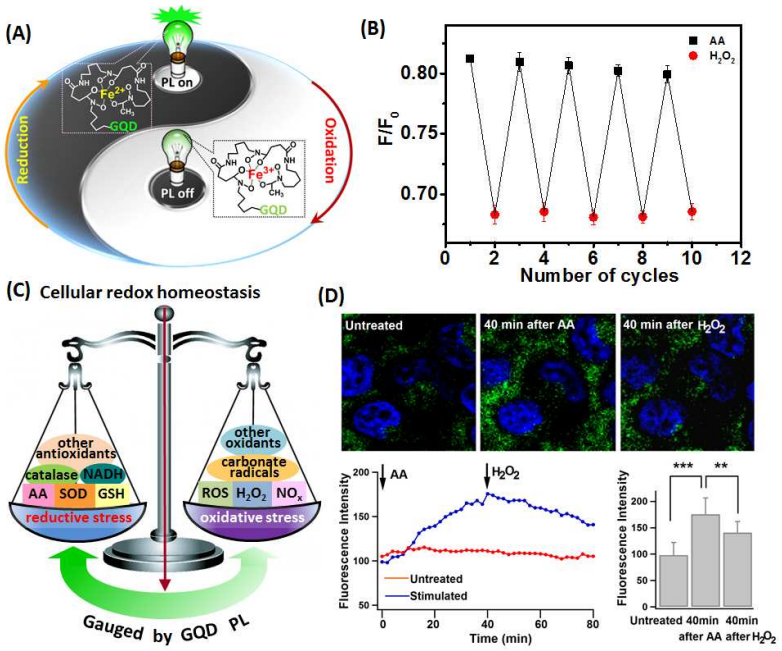

Figure 6. (A) Diagrammatic illustration of PL switching mechanism. (B) Reversible PL change induced by alternative addition of AA and H_2O_2. F_0 and F are PL intensities in the absence and presence of AA (10 μM) or H_2O_2 (10 μM). (C) Schematic illustration of cellular redox homeostasis and its monitoring by our GQD probe. (D) Dynamic monitoring of redox state in live Hela cells using GQD-DFOB-Fe^{3+}/Fe^{2+} probe under confocal microscopy. Top: confocal images. GQDs emit green fluorescence and nuclei are stained blue by NucBlue (Molecular Probes). Left at bottom: the time course of PL change (2 min interval). Arrows indicate the time points when the chemicals are added into the solution. Right at bottom: The statistics (mean ± standard deviation) of the fluorescence intensity of probe-loaded Hela cells (n = 12, taken at different field-of-view). Student's t-test: ***$p < 0.001$; **$p < 0.01$.

Table of Contents

A redox-sensitive fluorescence-switchable probe based on functionalized graphene quantum dots (GQDs) is designed for real-time monitoring dynamic changes of intracellular redox state in response to physiological stimuli.